International Journal of Nanoelectronics and Materials
Volume 15, No. 2, April 2022 [139-154]

Supercapacitor Performance with Activated Carbon and Graphene Aerogel Composite Electrodes

Abdul Hakim Ab. Rahim[1], Nabilah Ramli[1*], Anis Nurashikin Nordin[2] and Mohd. Firdaus Abd. Wahab[3]

[1]Department of Mechanical Engineering, Kulliyyah of Engineering, International Islamic University Malaysia, 53100, Kuala Lumpur, Malaysia
[2]Department of Electrical and Computer Engineering, Kulliyyah of Engineering, International Islamic University Malaysia, 53100, Kuala Lumpur, Malaysia
[3]Department of Biotechnology Engineering, Kulliyyah of Engineering, International Islamic University Malaysia, 53100, Kuala Lumpur, Malaysia

Received 20 November 2021, Revised 6 February 2022, Accepted 8 February 2022

ABSTRACT

Thus far, activated carbon (AC) has been the material of choice as practical supercapacitor electrode material. However, graphene can be a better alternative material. This work presents a comprehensive ratio study of AC and Graphene Aerogel (GA) as the sole and composite electrodes. The material and facile-fabricated electrodes were characterized, and the electrochemical performances of the prototypes were correlated and discussed in terms of specific capacitance, internal resistances, cyclic performance, and self-discharge. It was found that 20% GA addition on the AC electrode (GA20 specimen) recorded the highest charge-discharge specific capacitance at 78.9 F/g, which was 4% higher than AC at 75.8 F/g, even though the estimated surface area for the electrode was 20% lower than the pure AC electrode. Further addition of GA wt% decreased the capacitance due to the lack of electrode surface area. The equivalent series resistance (ESR) increased with an increase in GA wt% due to the higher electronic resistance of GA material. AC electrode had the lowest self-discharge among all specimens, which was caused by the deeper ion storage inside the electrode's pores.

Keywords: Graphene aerogel, activated carbon, supercapacitor, composite electrode, self-discharge

1. INTRODUCTION

Supercapacitors are a growing topic of interest, especially with the increase in appreciation of sustainable development visions. Its advantages of high-power delivery and long-life cycle motivate researchers to pursue a better energy density enhancement for supercapacitors. Composite approaches are being explored by combining the traditional activated carbon (AC) with many advanced carbons such as carbon nanotube or graphene, along with other options of metals and polymers. However, the hybrid material approach with a faradaic charge transfer mechanism can compromise the supercapacitor advantages and pure electric double layer mechanism can be achieved with carbon-carbon composites [1].

The supercapacitor's performance is rated based on its capacitance (Farads), its internal resistance or equivalent series resistance (Ω), and its operating voltage (Volts). Even though a supercapacitor theoretically has an almost unlimited life cycle, its actual life performance depends on the electrochemical setup and usage. Self-discharge occurrence in supercapacitors is a disadvantage that prevents the device from being used for energy-intense applications [2].

*Corresponding author: nabilah@iium.edu.my

These parameters are dependent on the properties of the electrode and electrolyte material used for the device.

An electrode contains an active material, which provides a highly accessible surface area to store ions, and an additive material, which acts as the conductivity enhancer for the electrodes and binder to form the electrode. Commercial supercapacitor devices can vastly be found using activated carbon (AC) as their electrode material, as it has a very high specific surface area (SSA); however, it is also known to have a non-uniform pore distribution and low conductivity [3]. On the other hand, graphene is a highly conductive material with a promising theoretical surface area. Graphene, which is a two-dimensional carbon sheet, can be assembled and tuned into several structures such as free-standing particles, one-dimensional fibers, two-dimensional films and even three-dimensional foams [4]. This causes the production cost of the material to be high and it is not yet feasible for large scale production. Furthermore, graphene sheets have a tendency to restack and agglomerate [5], which will reduce the effective surface area. 3D graphene such as Graphene Aerogel or Graphene Foam has the advantages of better pore structure and electrical conductivity over 2D graphene sheets, which can enhance surface utilization and ionic diffusion [6]. In addition to that, the possibility of graphene sheet restacking can be eliminated. Graphene Aerogel (GA), which is a three-dimensional (3D) graphene material, is an alternative for producing graphene-based supercapacitor and it can be prepared using many ways including oxidation-reduction, chemical vapor deposition and hydrothermal method. The hydrothermal process of producing the aerogel is the most common method where a graphene hydrogel is produced before being dried to become an aerogel [7]. Reducing graphene oxide (GO) promotes the self-assembly of graphene sheets into 3D structures. However, this method requires high temperature and more importantly, high pressure, where it is typically done in an autoclave machine, which produces the finished materials in batches rather than continuous production [8].

Alternatively, AC and graphene can be combined into composites to synergize the best of the two materials' properties. In this context, several works aimed to increase the electrode's performance by adding small amounts of graphene as an additive. Graphene Oxide (GO) was used in [9] in the electrode with AC synthesized from urea in 6M KOH electrolyte, where it was reported that the specific capacitance, C_{sp}, was 210 F/g, compared to the AC electrode from a commercial source with only 76 F/g, in a cyclic voltammetry (CV) test at 1 mV/s. Another work used only 2% multilayered graphene with their synthesized AC electrode from oil palm fruit bunch, where it produced a prototype with 45.72 F/g C_{sp}, which was five times higher than the AC electrode without graphene addition at 8.59 F/g [10]. For multiple ratios composite approach, a study varied the graphene wt% loading from 0 to 20 % and found out that using 8% reduced Graphene Oxide (rGO) as an additive for their AC electrode succeeded in increasing 5% of the C_{sp} to 215 F/g [11]. They used a cyclic charge-discharge method at 10 mA current and 6 M KOH electrolyte. More significant GO and KOH-activated carbon (KAC) ratios were used in [12] with GO:KAC of 0:1, 1:1, 1:2, and 1:3, respectively. Together with pure rGO, they were tested in 6 M KOH using 2 A/g current density charge-discharge. The prototypes reported specific capacitance of 126, 188, 205, 164, and 186 F/g, respectively. The 1:2 GO:KAC ratio achieved the highest C_{sp}, followed by the 1:1 composite and pure rGO, which can be attributed to their specific surface area (SSA) and pore distribution. A recent composite electrode approach varied Graphene Nanoplatelet (GNP) addition from 0% to 25% onto the AC electrode and analyzed the asymmetric composite ratio electrodes while mass balancing the positive and negative electrode to get the best prototype performance. They reported that 5% GNP addition on the positive and 15% GNP addition on the negative electrode, achieved 38 Wh/kg energy density and 149 kW/kg power density with a 1 M $TEABF_4$ in acetonitrile as the electrolyte [13]. While these reports indicated a graphene ratio limit to achieve the highest optimized electrode performance, our recent finding showed that the capacitance performance of AC-graphene composite electrodes was linearly related to the amount of electrode's mesoporous surface area [14].

However, studies on 3D graphene - AC composite electrodes can hardly be found, particularly regarding the comparison of the performance and the trade-offs between the two materials. This work investigates the use of the comprehensive ratios composite approach for an established material AC, a material with enormous SSA, and a GA material with a very low surface area but with a self-standing 3D graphene structure. The importance of the surface area based on the pore size is also highlighted in the findings. The paper starts with the characterization of the material used, followed by the fabrication and characterization of the electrodes as a supercapacitor device. The performance of the prototypes in terms of capacitance, internal resistance, cyclic performance, and self-discharge is reported and discussed.

In this paper, the experimental section presents the characterization of the raw materials used in this study, followed by a facile fabrication process of the electrode and the build of a supercapacitor cell based on comprehensive ratios such as those in [15]. It highlights the electrochemical performance of the prototype via Electrochemical Impedance Spectroscopy, Cyclic Voltammetry, Galvanostatic Charge Discharge and Open Circuit Voltage observation. The specimens' performance is correlated with the analyzed raw material properties in the discussion sections.

2. MATERIAL AND METHODS

First, material characterizations were done to identify the properties of the raw materials utilized in this work. Next, the composite electrodes were fabricated, followed by the specimen prototypes assembly. Then, the prototypes were characterized electrochemically to evaluate their performance as a supercapacitor device.

2.1 Characterization of materials

Commercial Graphene Aerogel (GA) was obtained from ACS Material. The GA was grounded using a Fritsch P4 planetary ball mill machine to produce GA powder. Activated carbon in the form of powder and 60 wt% PTFE-water solutions were acquired from Sigma-Aldrich while Carbon Black (CB) was obtained from Magna Value Sdn. Bhd. The powdered GA and the as-received AC structural graphitization were analyzed under Raman spectroscopy analysis using Renishaw in-Via Raman Microscope with 532 nm laser excitation. At the same time, the surface area and pore analysis was done using Brauner–Emmett–Teller (BET) and Barret–Joyner–Halenda (BJH) methods [16] via Micromeritics ASAP 2020 with MicroActive 2.0. The topological imaging of the raw material and electrode was done using the electron microscope (FESEM, Jeol JSM- 7800F Prime). The fabricated electrodes' electrical conductivity was tested under a two-points-probe using Keithley Parametric Analyzer SCS 400. The resistance measured solely depended on the composite ratio since the geometric of the electrodes were maintained.

2.2 Supercapacitor Electrode Fabrication and Device Assembly

Electrode specimens were produced according to the wt% shown in Figure 1(a), where AC and GA80 can be considered as pure controlled prototypes. PTFE was mixed with ethanol, which acted as a solvent. An ultrasonic homogenous mixer was used for PTFE dispersion continued by active materials powders addition before sonicated again homogeneously. The mixture was reduced to 10% of its original weight on a heating stirrer. The subsequent composite in the form of paste was divided equally as electrodes. The paste was formed on a Nickel mesh current collector using a 35 mm x 15 mm mold using a hydraulic press at 100 kPa. The active electrode material had a thickness of 1-1.5 mm. The prototype assembly schematics is shown in Figure 1(b). Two electrodes were separated by a microporous membrane separator of 25 μm thickness, where it was sandwiched between two 1 mm acrylic sheets which acted as housing. The sandwich was

immersed in 50 ml 6 M KOH bulk electrolyte inside a cylindrical specimen container. The container cap was punched to make way for the terminal and sealed using a hot glue gun to prevent electrolyte dehydration. Three sets of prototypes were fabricated using the three sets of GA acquired from the supplier.

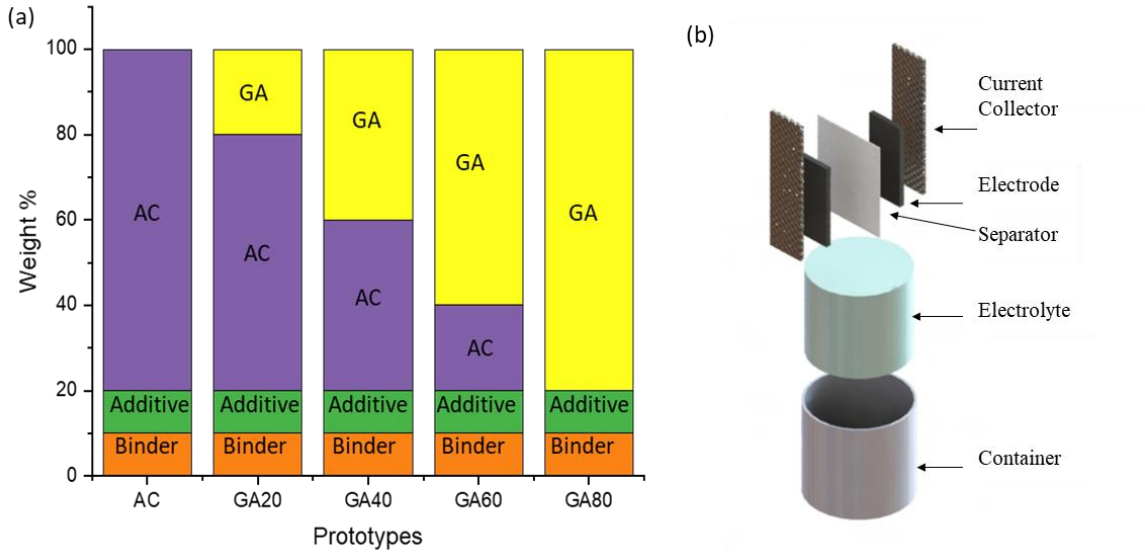

Figure 1: (a) The prototypes' composite ratio setup, (b) the assembled supercapacitor prototype schematics

2.3 Electrochemical Characterization

The assembled prototypes with two electrodes were characterized electrochemically using several methods. Electrochemical Impedance Spectroscopy (EIS) was carried out in a frequency range of 10 mHz to 10 MHz at an open-cell potential with 5mV alternating current perturbation. The specific capacitance, C_{sp} for the prototypes were measured from EIS using equation (1) [17]:

$$C_{sp} = -\frac{1}{\pi f_1 Z''_1 m} \quad (1)$$

where f_1 is the lowest frequency, Z''_1 is the imaginary impedance at f_1, while m is the weight of the electrodes. The electrode resistance, $R_{electrode}$, electrolyte resistance $R_{electrolyte}$, and the diffusion slope, $S_{diffusion}$, were obtained from the real axis of the Nyquist plot [18] as shown in Figure 2 .

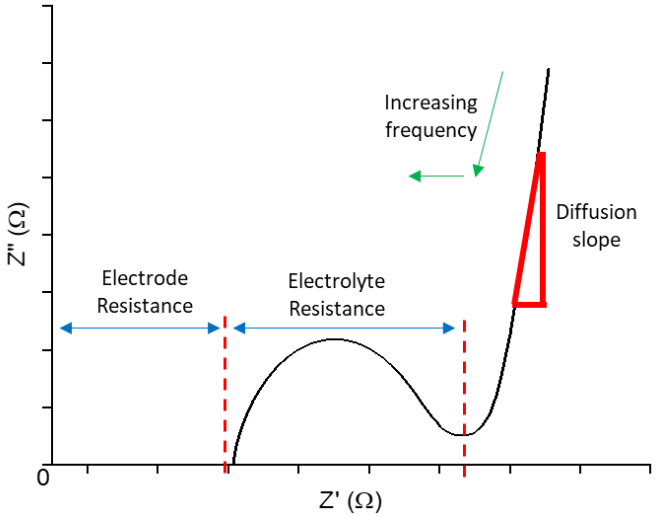

Figure 2: Parameters measured from the EIS Nyquist plot

Cyclic Voltammetry (CV) with scan rates of 1, 10, and 100 mV/s were observed in potential windows between 0 and 1 V. The C_{sp} for the prototypes were measured from CV using equation (2) [19]:

$$C_{sp} = \frac{Q}{\Delta V \; v \; m} \tag{2}$$

where Q is the area under the CV curve, ΔV is the potential window (V), while v is the scan rate (V/s). Both EIS and CV were measured using the Autolab PG302N Potentiostat. Neware Battery Testing System (BTS) 5V100mA was used for Galvanostatic Charge-Discharge (GCD) with constant current of 4, 8, and 12 mA. The cyclic performance was carried out for 900 cycles using a constant current of 10 mA. Open Circuit Voltage (OCV) was measured for 3600 seconds after the prototypes were charged at 1 V using 10 mA current. The C_{sp} was measured from GCD using equation (3) [2]:

$$C_{sp} = \frac{4 \; I \; \Delta t}{\Delta V \; m} \tag{3}$$

with I as the discharge current (A) and Δt as the discharge time (s). The equivalent series resistance (ESR) acquired from the GCD test was calculated by dividing the voltage drop that was generated between charging and discharging with the change in the current [20].

3. RESULTS AND DISCUSSION

3.1 Material Characterization

3.1.1 Surface Area and Pore Analysis

According to the IUPAC technical report, the physisorption profile for AC in Figure 3(a) can be categorized as a class II isotherm with a H4 hysteresis form, which shows that AC contains pores in micro-meso structured forms. The GA profile in Figure 3(b), on the other hand, adsorbed a much lower adsorbent (N_2 gas) quantity during the whole testing. The profile did not match any of the six isotherm classifications but did show a hysteresis pattern, which confirms the existence of mesopores in GA [21].

The BET surface analysis indicates that the overall surface area of AC was estimated to be at 1038.55 m^2/g, which is almost 80 times higher than GA at only 13.5 m^2/g. Using the BJH adsorption/desorption analysis, the pores within 1.7 nm and 300 nm (mesopores + macropores) range for both materials were much lower, with 361.88 m^2/g for AC and only 2.85 m^2/g for GA. This result was used to estimate the total SSA for each prototype shown in Table 1, which are mapped in Figure 9(b) for performance comparison. Since the SSA difference between the two active materials was very large, the trend of the electrodes' surface area estimation was a steep decrease as the GA wt% increased. The SSA estimated for the pure GA80 prototype implied the presence of only a few m^2/g of surface areas since the weight of the electrodes was less than 1 gram.

Table 1: Specific Surface Area estimation for electrode composites

Electrodes (GA %wt)	BET (m^2/g)	BJH (m^2/g)
0	830.40	165.90
20	623.47	124.52
40	416.54	83.15
60	209.61	41.77
80	2.68	0.39

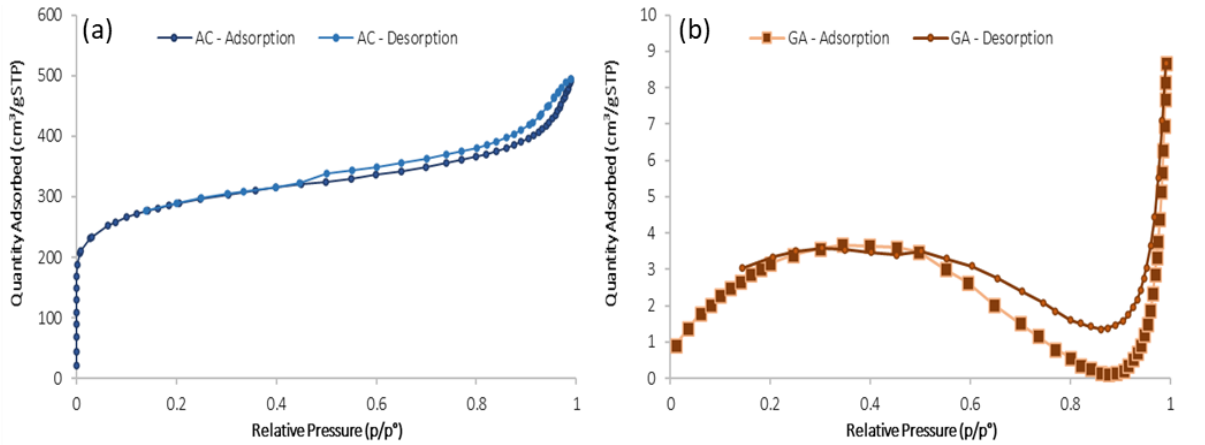

Figure 3: (a) Physisorption for AC particles, (b) physisorption of GA

3.1.2 Raman Spectroscopy

In the Raman spectrum of the materials in Figure 4, both materials had distinguishable D band and G band peaks, implying that the materials had amorphous/crystalline properties. GA had higher D and G band intensity at 1061 and 906 a.u while AC was at 882 and 711 a.u. The shape of the GA spectra implied a reduced-graphene oxide (rGO) shape with a D band higher than the G band [22]. Higher intensity ratios from the D band to G band (I_D/I_G) were seen for AC at 1.23 compared to GA at 1.17, indicating that AC had a higher degree of structural disorder.

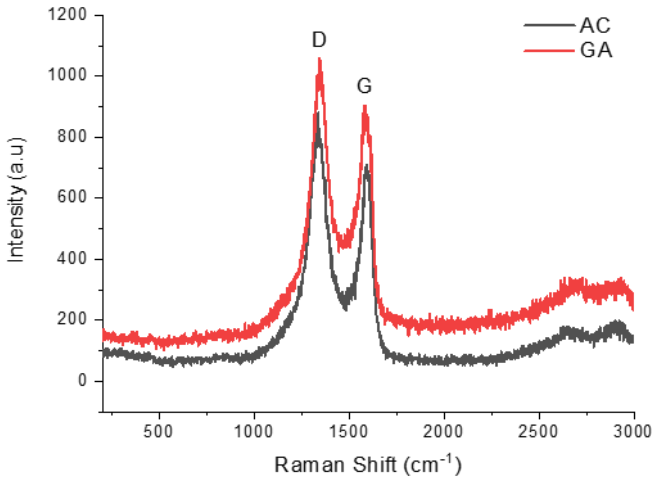

Figure 4: Raman spectrum of AC and GA materials

3.1.3 Two Points Probe

The resistance of the electrodes is shown in Figure 5, and it can be seen to be increasing with increasing GA wt%, where the GA80 electrode reached almost 1200 Ω/cm. This reveals that the GA particles had a lower electrical conductivity compared to AC.

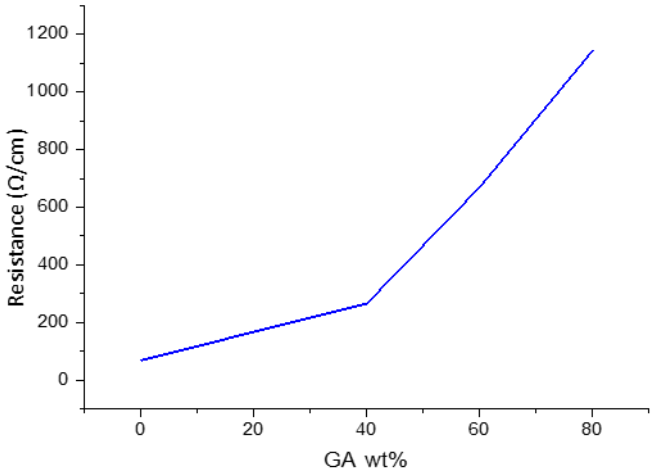

Figure 5: Electrical resistance of the composite electrodes

3.1.4 Scanning electron microscopic imaging

SEM images of the active materials can be seen in Figure 6. The AC's particle surface in Figure 6(a) has an unsymmetrical wavy shape, while the grounded GA in Figure 6(b) had a shape with a few layers of graphene flakes with intact porosity after grounding. The size of the AC particles was much larger compared to the GA particles. Fabricated electrodes of the GA20 composite electrode are presented in Figure 6(c), while the GA80 electrode is in Figure 6(d). All the materials were mixed adequately with CB and binder PTFE.

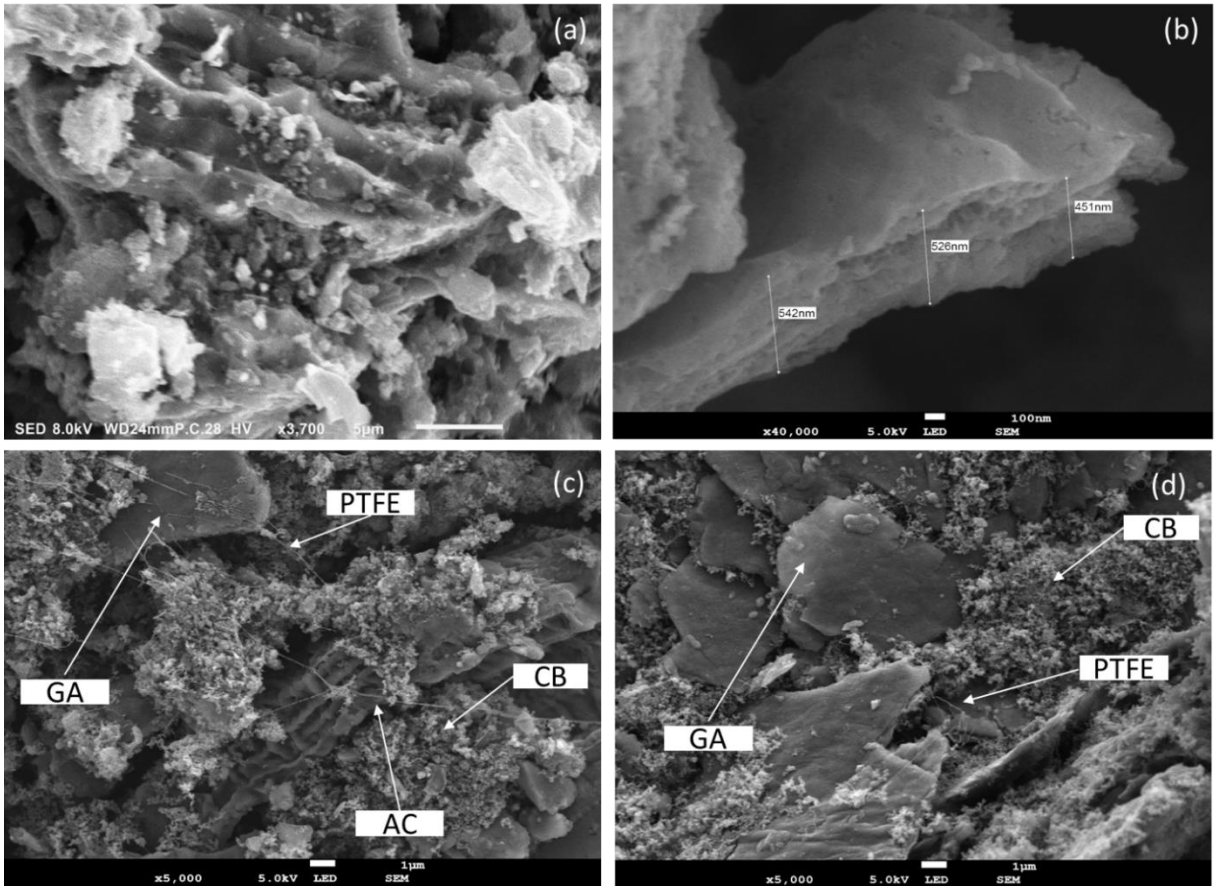

Figure 6: SEM images for (a) AC, (b) GA powder, (c) GA20 electrode and (d) GA80 electrode

3.2 Electrochemical Characterization

3.2.1 Electrochemical Impedance Spectroscopy

The Nyquist plot for all prototypes is shown in Figure 7(a). Generally, prototypes with higher GA wt% resulted in larger semi-circle loops. The C_{sp} acquired from the plot is compared in Figure 7(b). The subsequent resistances proposed by [18], namely the electrode resistance, $R_{electrode}$, and electrolyte resistance, $R_{electrolyte}$, were also extracted from the plot and presented in Figure 7(b).

It can be seen that C_{sp} have a decreasing trend in general with the increase in GA wt% from 17.6 F/g for AC to 7.7 F/g for GA80. However, GA20 is an exception where the 20% GA addition on the AC electrode had increased the C_{sp} by 6% to 18.7 F/g. $R_{electrode}$ had a resistance of 2 to 3 Ohms for all prototypes without any particular trend. However, $R_{electrolyte}$ demonstrated an increasing resistance value with higher GA wt%. $S_{diffusion}$ also showed an increasing trend but in a low and steady slope. The EIS result suggests a different reason for the obtained resistance values compared to the one proposed in [18]. $R_{electrode}$ was stable despite the difference in the electrode's electronic resistance, which suggests that the initial impedance in the Nyquist plot was due to a standardized arrangement of all prototypes, such as the current collector–electrode interface. Instead, the similar trend of $R_{electrolyte}$ and the electrical resistance outcome in Figure 5 reveals a relationship between the electrode electrical conductivity and the second R in the Nyquist plot. Even though all prototypes were using the same electrolyte, the more conductive electrode would emit a higher electric field, thus influencing the electrolyte's ionic movements and resulting in a lower ionic resistance.

It can be noted that a greater slope for $S_{diffusion}$ indicates more electric double layer (EDL) formation on the electrode-electrolyte interface, while a smaller slope suggests that the charging mechanism

was under ionic diffusion influence [18]. The $S_{diffusion}$ trend is shown in Figure 12, where it was compared with the diffusion activity observed from the self-discharge method.

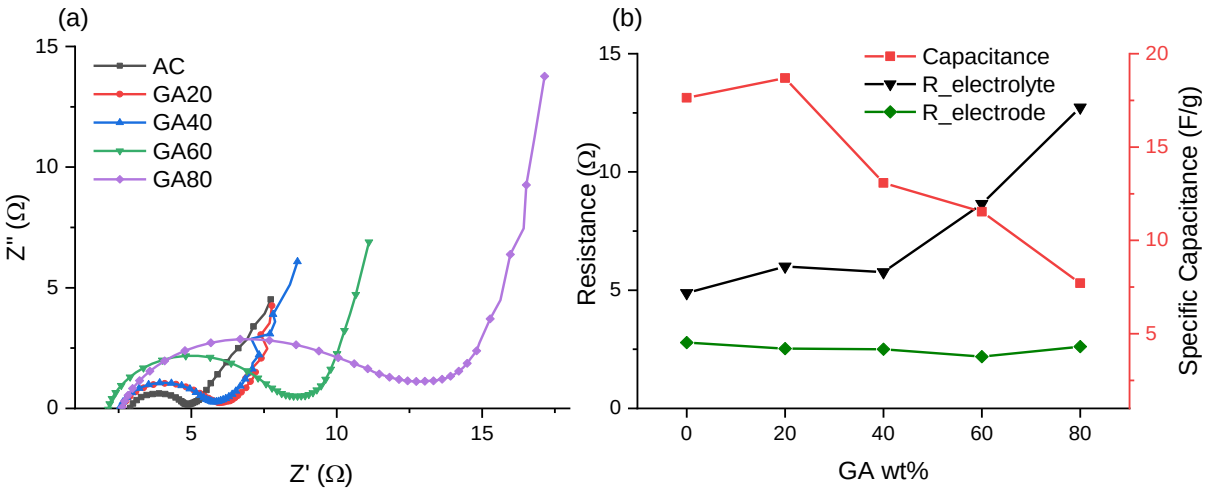

Figure 7: (a) Nyquist plot for all prototypes, (b) the specific capacitance, electrode and electrolyte resistance, and diffusion slope measured from the Nyquist plot

3.2.2 Cyclic Voltammetry

The CV profiles indicated good electrochemical stability for all prototypes between 0 to 1 V as shown in Figure 8. Leaf-shaped curves were seen for 0.001 V/s, with the AC plot illustrating the most significant area under the curve, while GA80 had the smallest area. Higher scan rates resulted in smaller curves and the shape had changed to more quasi-rectangular shapes as seen from Figure 8(a) to (c), which implied higher resistances. At medium and high scan rates, the performance of the AC prototypes worsened to the thinnest curve. The plot area represents charges that were stored in the electrode during the exercise. The resulting capacitances are presented in Figure 8(d).

At a low scan rate, AC had the highest C_{sp}, with a decreasing C_{sp} trend as the GA wt% increased. However, at a medium scan rate, AC could not capture more ions quickly, hence AC performed the worst among the prototypes. This observation could be influenced by the micropores of the AC, which is beneficial during slow charging as the ions have ample time to move inside the micropores, but are constrained in quicker charging. All prototypes could not store significant charges at the highest scan rate due to the high material loading on the current collector. The electrode pores could not abide by the high voltage perturbation which caused asynchronous charging [23], where only the outer surface of the electrodes managed to store the ions.

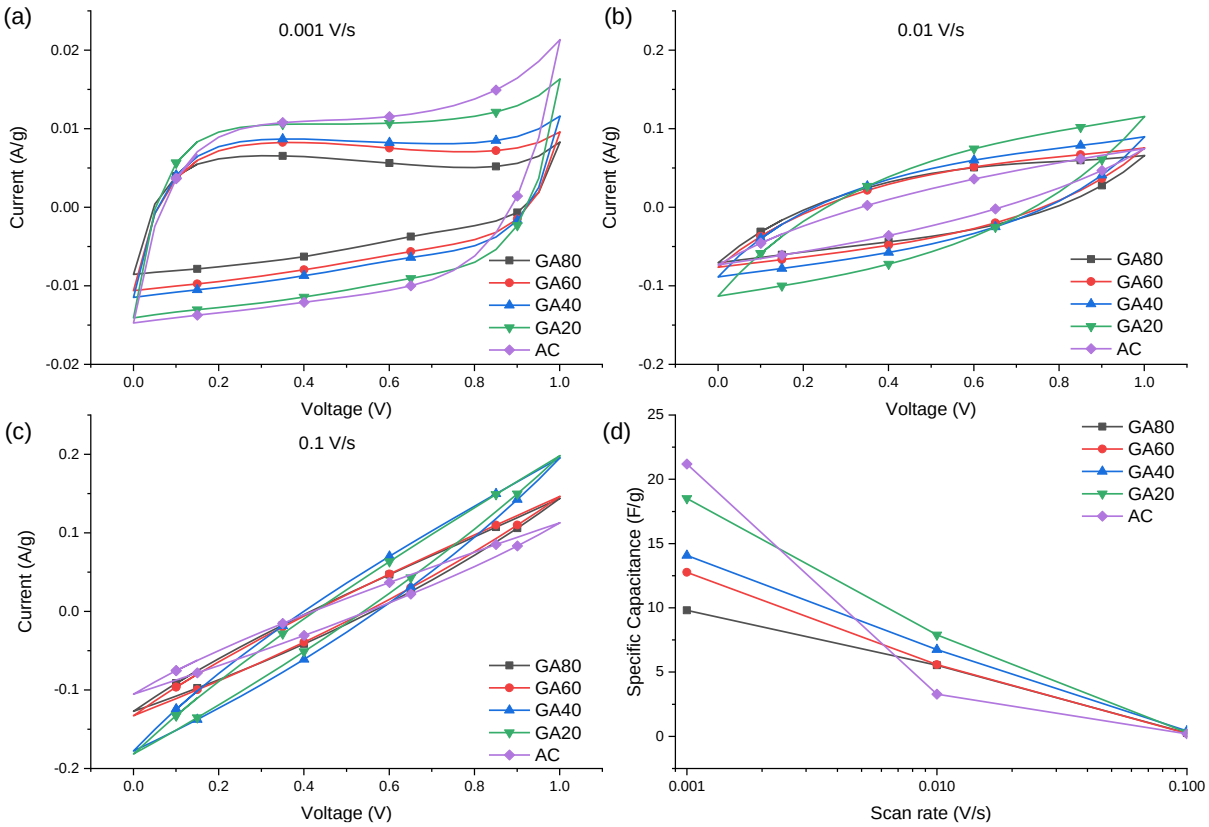

Figure 8: Cyclic Voltammetry curves for all prototypes under (a) 0.001 V/s, (b) 0.01 V/s, (c) 0.1 V/s and (d) the respective specific capacitance

3.2.3 Galvanostatic Charge Discharge

The GCD profile for all prototypes under a constant current of 4 mA is shown in Figure 9(a). All C_{sp} values are compared in Figure 9(b) for current values of 4, 8, and 12 mA. As anticipated, the C_{sp} decreased with an increase in GA wt% in general, since the surface area of GA was very low compared to AC, which can be cross-referenced in Figure 9(b). However, the GA20 prototype had a slight C_{sp} improvement of 4% at 78.9 F/g for low current and it is a comparable performance with the AC prototype in medium and high current. For composite prototypes with higher GA addition, a clear trend of C_{sp} decrement was observed, similar to the BJH surface area estimation. The ESR recorded for all prototypes is presented in Figure 9(c).

20% addition of GA improved the charging-discharging mechanism of the AC prototype, even though the surface area of the electrode was lower than the pure AC electrode. The improvement was not due to better electrode conductivity since the ESR reported a consistent trend of electronic resistance increment. On the other hand, the improvement could be due to optimized pore accessibility since the two materials had different shape, pore sizes and distributions. More ions could reside on the electrode particle surfaces, thus resulting in higher capacitance turnover.

Lower capacitance performances were recorded for GA addition of more than 20%. This is clearly due to the lower available surface area for the ions to interact with. The GA used in this work had very low SSA compared to those in recently reported works in the literature. Different performances may be seen for this approach if GA with high SSA is used. The C_{sp} standard deviation bar increased with increasing GA as different sets of prototypes came from different raw material batches. The performance inconsistency highlights another disadvantage of GA as the product can only be produced in small-scale batches. The comparison in terms of capacitance values with other carbon-graphene composite prototypes reported in the literature is tabulated in Table 2.

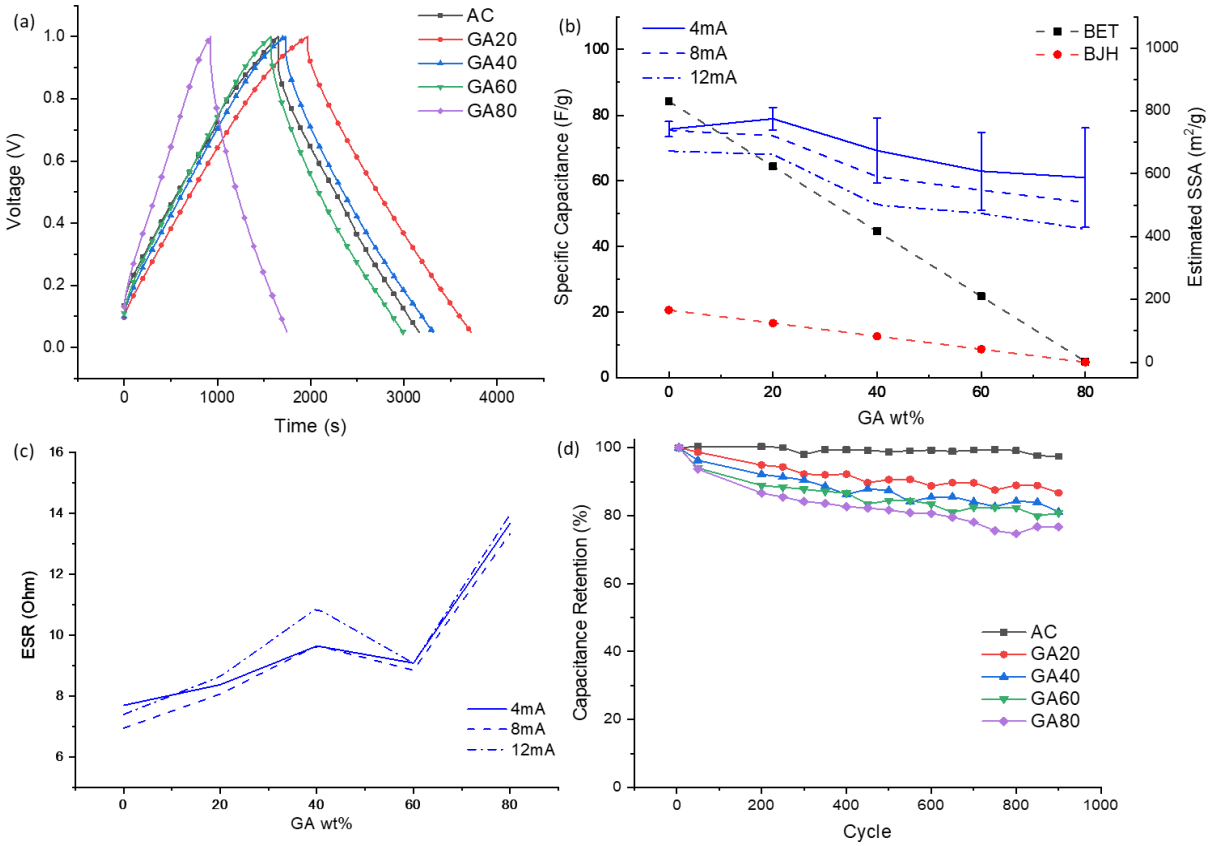

Figure 9: (a) charge-discharge profiles of all prototypes, (b) specific capacitance under different currents vs. estimated specific surface area for all electrodes, (c) the ESR, and (d) life performance for 900 cycles

After 900 cycles, the capacitance retention for all prototypes can be seen to reduce in a linear trend, as shown in Figure 9(d). The AC prototype maintained its performance at 97.4 %, while GA80 deteriorated to 76.7%. The GA80 and AC electrodes morphology before and after the cyclic exercise are displayed in Figure 10. The edges of the cycled GA particles were damaged and broken, hence resulting in a lower effective surface area. As the GA particles were not very conductive, the constant current moving in and out would induce thermal stress and damaged the graphene edges and layers [1], [27]. The KOH that was used as the electrolyte was also known for carbon pores activation and alteration [28], and its eroding capability could be a contributing factor in boosting the damages as the GA particles were thinner than the AC particles. This finding is similar to a reported work that was using another type of graphene [14].

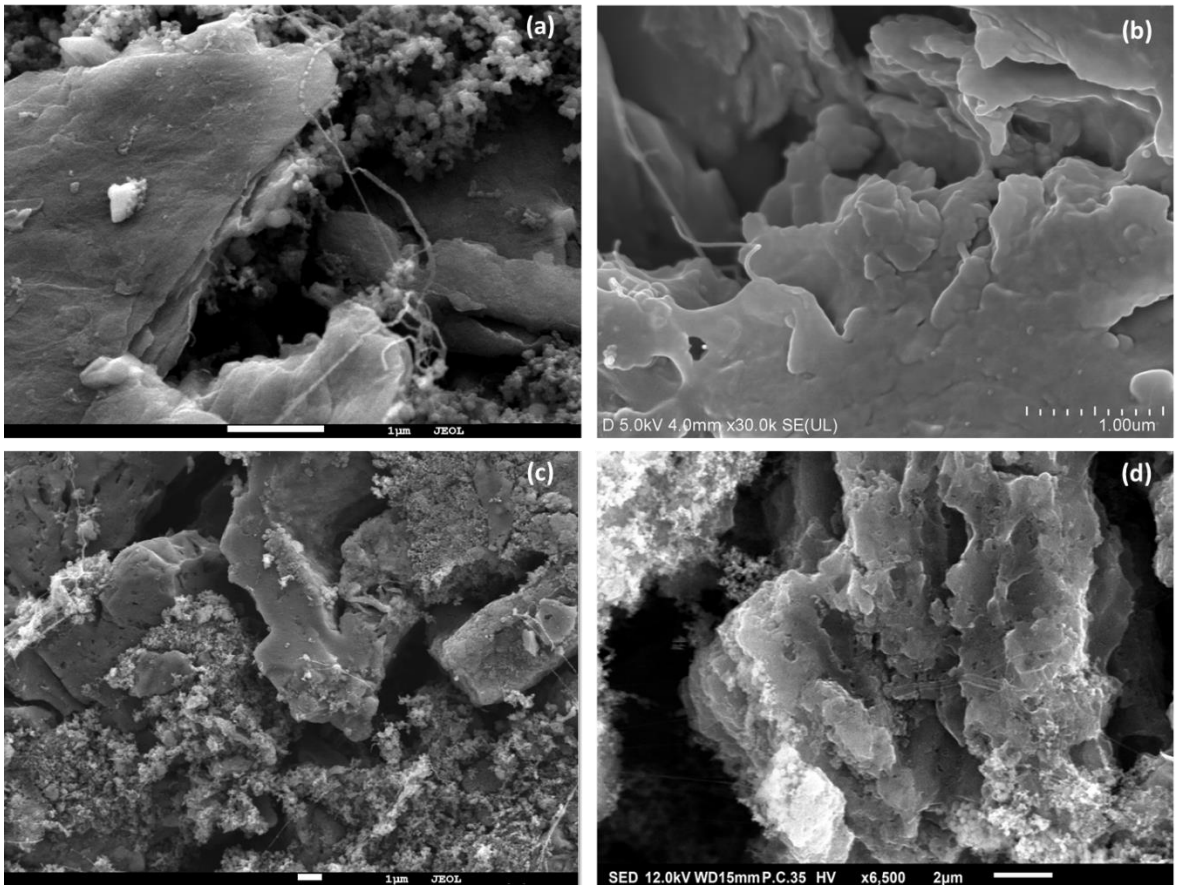

Figure 10: SEM images of (a) the fresh and (b) cycled GA80 electrode, (c) the fresh and (d) cycled AC electrode

Table 2: Capacitance values of carbon-graphene composites electrode material

Material	Capacitance (F/g)	Reference
Activated carbon / few layers graphene (1:4)	587	[24]
Activated carbon/graphene hybrid aerogel	294	[25]
Activated carbon / reduced Graphene oxide (8%)	215	[11]
Activated carbon / Graphene oxide	210	[9]
Reduced Graphene Oxide / KOH-Activated carbon (1:2)	205	[12]
Activated carbon / Graphene Aerogel (20%) (present work)	78.9	-
Graphene-coated Carbon Nanotube	60-110	[26]
Activated carbon / multilayered graphene (2%)	45.7	[10]

3.2.4 Self-discharge

The Open Circuit Voltage procedure resulted in an almost similar trend with the C_{sp} performance. The self-discharge in voltage percentage profile is shown in Figure 11(a). The self-discharge profile

can be studied to determine faradaic reactions occurrence, ohmic leakage, and charge redistribution [29], [30], which can characteristically be seen as a linear plot in the *V vs. Log t*, *Ln V vs. t*, and *V vs.* $t^{1/2}$ graphs, respectively. These plots are presented in Figure 11(b), (c) and (d).

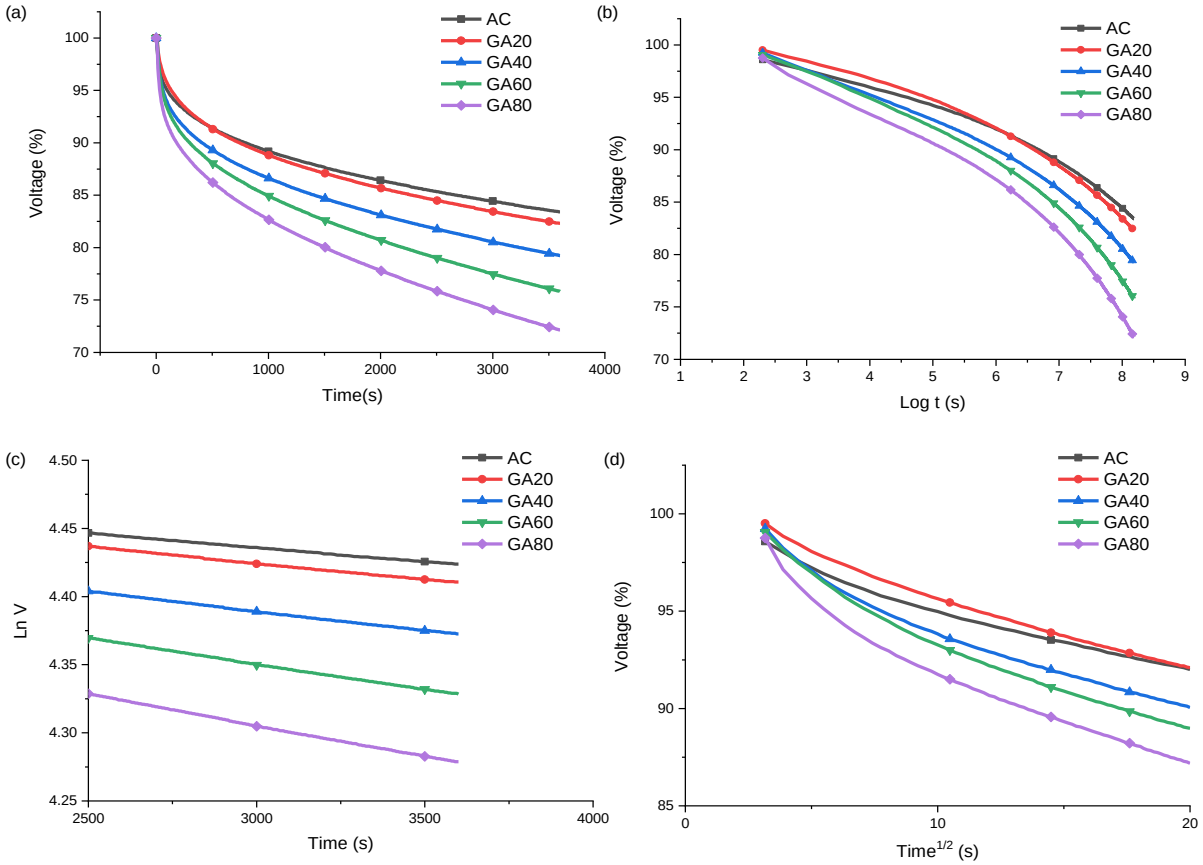

Figure 11: (a) Self-discharge profiles of prototypes, and profiling the self-discharge due to (b) faradaic reaction, (c) ohmic leakage, and (d) charge redistribution

As the potential window limit of the KOH electrolyte was observed during charging-discharging procedures, no faradaic reaction is expected to happen on the prototypes due to electrolyte decomposition as proven in the CV test. Figure 11(b) shows no linear correlation between *V* and *Log t*, hence confirming that the pure EDLC charge storage mechanism was without any faradaic reaction presence. The ohmic leakage plot at the final 500 seconds in Figure 11(c) shows a linear connection between *Ln V* and *t*, thus proving that there was current leakage through ohmic resistance, which was induced by the prototype assembly setup.

For the charge redistribution profile in Figure 11(d), there were no prominent straight and linearly declining profiles, which were anticipated to be present as proof of ionic rearrangement. This may be due to the mixed indication with the high ohmic leakage [2]. A considerable drop can be seen from the AC profile before the more gradual slope. This shows that a significant portion of ions were diffused quickly during the early phase of charge redistribution. This implies that those ions were unable to penetrate the deeper pores and were only stored at the outer pore surface of the electrode since AC had many micropores. However, in general, the charge redistribution's sloping trend can be seen to increase from AC to GA80, as shown in Figure 12. A higher slope is caused by higher ionic diffusion concentration; thus, more ions will be redistributed during the relax time [22]. The increasing diffusion trend for the self-discharge method is similar to the $S_{diffusion}$ result from EIS, but the interpretation is different. From both EIS and self-discharge test, it can be concluded that a

higher GA wt% encourages the occurrence of double-layer charging since the ions can penetrate the pores easier and be adsorbed on the surface of the electrode. In addition to that, there are more flat surface compositions with higher GA wt% for the diffuse charging activity to take place.

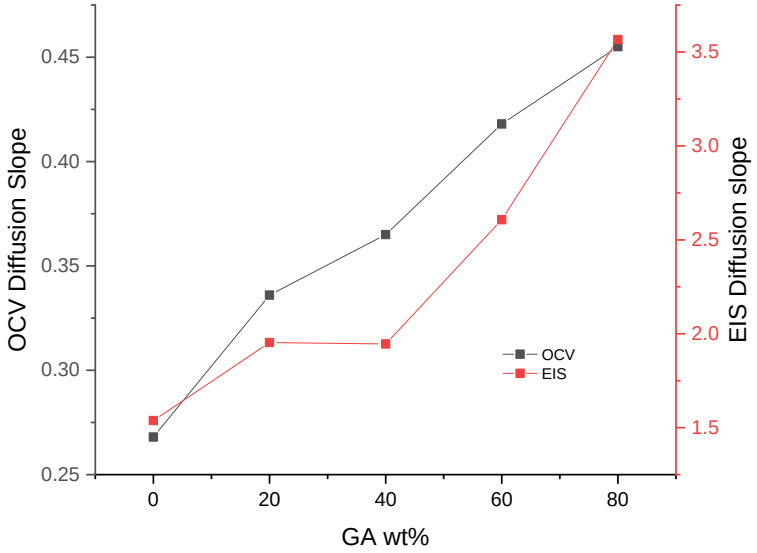

Figure 12: Diffusion activity comparison according to EIS and Self-discharge procedure

4. CONCLUSION

The paper presented a comprehensive analysis of the performance of AC-GA composite electrodes. A 3D graphene and AC composite electrode fabricated using the slurry and mold pressing method was reported for the first time in this study. AC, which is the traditionally used material, contains 80 times higher specific surface area and better electronic conductivity than GA, which is a 3D graphene type of material.

It was found that 20% GA addition on the AC electrode increased the specific capacitance by 4% in the low current setup, even though the estimated BJH surface area decreased by 25%. The improvements indicate that more ions can access the electrode pores with the assistance of GA. Further addition of GA continued to decrease the specific capacitance due to the inadequate surface area for the ions to reside. The ESR of the prototypes also increased with increasing GA wt%, following the increase in electronic resistance of the electrodes. The cyclic performance of the AC prototype was still maintained after 900 cycles, while higher deterioration occurred with higher GA wt% addition. A similar trend can be seen for the self-discharge performance where prototypes with higher GA wt% lost more charge within 3600 seconds due to the higher charge redistribution activity.

From the EIS and self-discharge procedure, it was found that the addition of GA increased both double-layer and diffusion charging on the electrode since the pores of GA were flat and easier to be accessed by the ions. This should be beneficial in increasing the power density of the prototypes. The performance of electrodes using GA with SSA that is higher than AC will be reported in future work.

ACKNOWLEDGEMENTS

The authors would like to thank Prof. Dr. Raihan (IIUM) for allowing the use of the Energy lab equipment and facilities, and AOARD (FA2386-18-1-4048) for the funding of this study.

REFERENCES

[1] S. Liu, L. Wei, and H. Wang, "Review on reliability of supercapacitors in energy storage applications," *Appl. Energy*, vol. 278, no. August, 2020.
[2] S. Subramanian, M. A. Johny, M. Malamal Neelanchery, and S. Ansari, "Self-Discharge and Voltage Recovery in Graphene Supercapacitors," *IEEE Trans. Power Electron.*, vol. 33, no. 12, pp. 10410–10418, Dec. 2018.
[3] K. V. G. Raghavendra *et al.*, "An intuitive review of supercapacitors with recent progress and novel device applications," *J. Energy Storage*, vol. 31, no. April, p. 101652, 2020.
[4] Q. Ke and J. Wang, "Graphene-based Materials for Supercapacitor Electrodes - A Review," *J. Mater.*, vol. 2, no. 1, pp. 37–54, Jan. 2016.
[5] R. Atif and F. Inam, "Reasons and remedies for the agglomeration of multilayered graphene and carbon nanotubes in polymers," *Beilstein J. Nanotechnol.*, vol. 7, no. 1, pp. 1174–1196, 2016.
[6] Z. Wang, H. Gao, Q. Zhang, Y. Liu, J. Chen, and Z. Guo, "Recent Advances in 3D Graphene Architectures and Their Composites for Energy Storage Applications," *Small*, vol. 15, no. 3, pp. 1–21, 2019.
[7] G. Gorgolis and C. Galiotis, "Graphene aerogels: A review," *2D Materials*, vol. 4, no. 3. 2017.
[8] J. Mao, J. Iocozzia, J. Huang, K. Meng, Y. Lai, and Z. Lin, "Graphene aerogels for efficient energy storage and conversion," *Energy Environ. Sci.*, vol. 11, no. 4, pp. 772–799, 2018.
[9] C. Zheng, X. Zhou, H. Cao, G. Wang, and Z. Liu, "Synthesis of porous graphene/activated carbon composite with high packing density and large specific surface area for supercapacitor electrode material," *J. Power Sources*, vol. 258, pp. 290–296, 2014.
[10] M. Deraman *et al.*, "Graphene and Activated Carbon Based Supercapacitor Electrodes," *Adv. Mater. Res.*, vol. 1112, no. July, pp. 231–235, 2015.
[11] S. Zhang, C. Lum, and N. Pan, "Enhanced performance of carbon/carbon supercapacitors upon graphene addition," *Nanotechnol. Environ. Eng.*, vol. 2, no. 1, pp. 1–8, 2017.
[12] S. Yu, Y. Li, and N. Pan, "KOH activated carbon/graphene nanosheets composites as high performance electrode materials in supercapacitors," *RSC Adv.*, vol. 4, no. 90, pp. 48758–48764, 2014.
[13] E. Redondo, L. W. L. Fevre, R. Fields, R. Todd, A. J. Forsyth, and R. A. W. Dryfe, "Enhancing supercapacitor energy density by mass-balancing of graphene composite electrodes," *Electrochim. Acta*, vol. 360, no. October, 2020.
[14] A. H. Ab. Rahim, N. Ramli, A. N. Nordin, and M. F. Abd. Wahab, "Supercapacitor performance with Activated Carbon and Graphene Nanoplatelets composite electrodes, and insights from the Equivalent Circuit Model," *Carbon Trends*, vol. 5, p. 100101, 2021.
[15] R. N. A. R. Seman and M. A. Azam, "Hybrid heterostructures of graphene and molybdenum disulfide: The structural characterization and its supercapacitive performance in 6M KOH electrolyte," *Journal of Science: Advanced Materials and Devices*, vol. 5, no. 4. pp. 554–559, 2020.
[16] R. Bardestani, G. S. Patience, and S. Kaliaguine, "Experimental methods in chemical engineering: specific surface area and pore size distribution measurements—BET, BJH, and DFT," *Can. J. Chem. Eng.*, vol. 97, no. 11, pp. 2781–2791, 2019.
[17] E. Hamdan *et al.*, "Electrochemical impedance spectroscopy study of carbon electrodes prepared from date pits and fibers of oil palm empty fruit bunches," in *AIP Conference Proceedings*, 2016, vol. 1784, p. 040008.
[18] B. A. Mei, O. Munteshari, J. Lau, B. Dunn, and L. Pilon, "Physical Interpretations of Nyquist Plots for EDLC Electrodes and Devices," *J. Phys. Chem. C*, vol. 122, no. 1, pp. 194–206, 2018.

[19] C. Zequine *et al.*, "High per formance and flexible supercapacitors based on carbonized bamboo fibers for wide temperature applications," *Sci. Rep.*, vol. 6, no. July, pp. 1–10, 2016.
[20] N. Blomquist, T. Wells, B. Andres, J. Bäckström, S. Forsberg, and H. Olin, "Metal-free supercapacitor with aqueous electrolyte and low-cost carbon materials," *Sci. Rep.*, vol. 7, p. 39836, Jan. 2017.
[21] M. Thommes *et al.*, "Physisorption of gases, with special reference to the evaluation of surface area and pore size distribution (IUPAC Technical Report)," 2015.
[22] I. Childres, L. A. Jauregui, W. Park, H. Caoa, and Y. P. Chena, "Raman spectroscopy of graphene and related materials," *New Dev. Phot. Mater. Res.*, pp. 403–418, 2013.
[23] S. Fletcher, V. J. Black, and I. Kirkpatrick, "A universal equivalent circuit for carbon-based supercapacitors," *J. Solid State Electrochem.*, vol. 18, no. 5, pp. 1377–1387, May 2014.
[24] M. Mandal, S. Subudhi, I. Alam, B. Subramanyam, S. Patra, and P. Mahanandia, "Simple and cost-effective synthesis of activated carbon@few layers of graphene composite electrode for supercapacitor applications," *IOP Conf. Ser. Mater. Sci. Eng.*, vol. 1166, no. 1, p. 012007, 2021.
[25] Q. Zhu, L. Ma, H. Wang, M. Jia, Y. Guan, and B. Xu, "Activated Carbon / Graphene Hybrid Aerogels as Electrode Materials for High Performance Supercapacitors," *ChemistrySelect*, vol. 2, no. 16, pp. 4456–4461, 2017.
[26] E. Wilson and M. F. Islam, "Ultracompressible, high-rate supercapacitors from graphene-coated carbon nanotube aerogels," *ACS Appl. Mater. Interfaces*, vol. 7, no. 9, pp. 5612–5618, 2015.
[27] Y. Huang and G. Zhao, "Preparation and characterization of activated carbon fibers from liquefied wood by KOH activation," *Holzforschung*, vol. 70, no. 3, pp. 195–202, 2016.
[28] H. M. Yang, D. H. Zhang, Y. Chen, M. J. Ran, and J. C. Gu, "Study on the application of KOH to produce activated carbon to realize the utilization of distiller's grains," *IOP Conf. Ser. Earth Environ. Sci.*, vol. 69, no. 1, 2017.
[29] B. W. W. Ricketts and C. Ton-That, "Self-discharge of carbon-based supercapacitors with organic electrolytes," *J. Power Sources*, vol. 89, no. 1, pp. 64–69, 2000.
[30] H. A. Andreas, "Self-Discharge in Electrochemical Capacitors: A Perspective Article," *J. Electrochem. Soc.*, vol. 162, no. 5, pp. 5047–5053, Jan. 2015.